iScience

CellPress
OPEN ACCESS

Article

Electrothermally tunable terahertz cross-shaped metamaterial for opto-logic operation characteristics

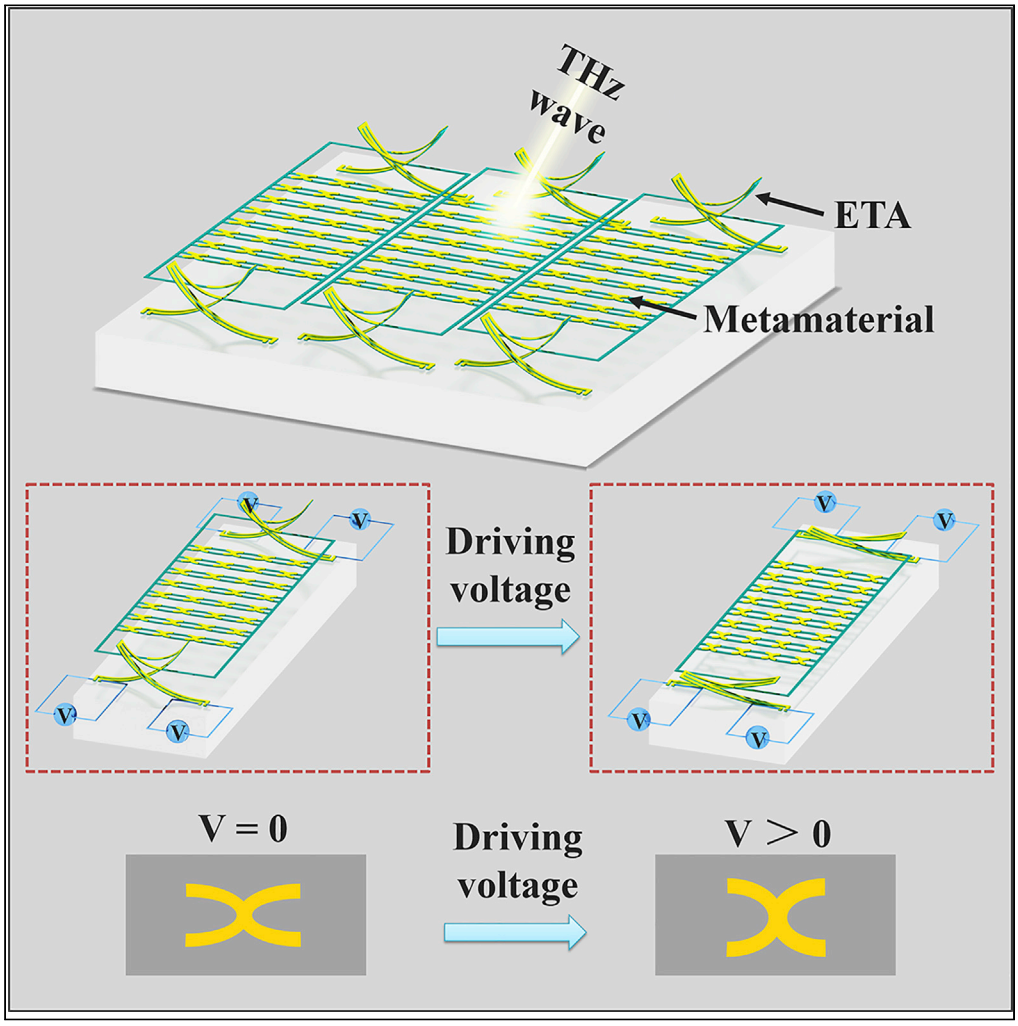

Ruijia Xu, Xiaocan Xu, Yu-Sheng Lin

linyoush@mail.sysu.edu.cn

Highlights

MEMS-based metamaterial is used to perform the opto-logic function

When driving a DC bias voltage of 0.20 V, the tuning range is 0.54 THz

"XNOR" logic gate function can be realized at 1.20 THz

Xu et al., iScience *25*, 104072
April 15, 2022 © 2022
https://doi.org/10.1016/j.isci.2022.104072

iScience

CellPress
OPEN ACCESS

Article

Electrothermally tunable terahertz cross-shaped metamaterial for opto-logic operation characteristics

Ruijia Xu,[1] Xiaocan Xu,[1] and Yu-Sheng Lin[1,2,*]

SUMMARY

We propose and demonstrate a metamaterial design by integrating a microelectromechanical system (MEMS) electrothermal actuator (ETA) platform and a cross-shaped metamaterial (CSM) to perform opto-logic function characteristics. Reconfigurable and stretchable mechanisms of CSM are achieved by driving different DC bias voltages on ETA to improve the limitations induced by the conventional use of the flexible substrate. The optical responses of CSM are tunable by the electrical signals inputs. By driving a DC bias voltage of 0.20 V, a tuning range of CSM is 0.54 THz is obtained and it and provides perfect zero-transmission characteristics. In addition, the "XNOR" logic gate function of CSM is realized at 1.20 THz, which plays a key role in the all opto-logic network communication system. The proposed MEMS-based CSM exhibits potential applications in logical operation, signal modulation, optical switching, THz imaging, and so on.

INTRODUCTION

Over the past few decades, metamaterials have attracted extensive attention for their unique characteristics that allow people to control the electromagnetic wave by properly tailoring the geometrical dimensions (Landy et al., 2008; Liu et al., 2010; Ma and Cui, 2010). Metamaterials have enabled a wide variety of applications, including invisibility cloaks, negative refraction indices, energy harvesters, and so on (Das et al., 2021; Kim et al., 2021). They have been demonstrated through the electromagnetic spectra from microwave to visual light (Chen et al., 2009; Xu and Lin, 2020; Xu et al., 2020; Zheng and Lin, 2020). Among these devices, terahertz (THz) metamaterial device has become a research hotspot and plays an essential role in accelerating the development of THz wave-based optoelectronic devices. Because THz metamaterials exhibit extraordinary electromagnetic properties that natural materials cannot realize, they have been widely reported in the implantations of modulators, sensors, and detectors (Lee et al., 2012; Tao et al., 2008). Although many THz metamaterials have been demonstrated with the powerful performances, they cannot be actively tuned once fabricated on the rigid substrates (Chen et al., 2010). THz electromagnetic responses of metamaterials are strongly dependent on the geometry and arrangement of periodic unit cells. To control metamaterials and achieve tunable responses, various approaches are developed by modifying the propagation of THz waves. To achieve the dynamic THz metamaterial, the conventional method is driving an external stimulus to modulate the metamaterials electromagnetic properties, including thermal annealing, phase changing, photo excitation, and light-controlled (Kenanakis et al., 2014; Liu et al., 2012; Xu and Lin, 2019; Zhang et al., 2018a; Zhang et al., 2020a, 2020b; Zhang et al., 2018b). Such methods suffer from the limitation of tuning range because of the intrinsic properties of natural materials. To avoid such limitations, another strategy is raised to directly change the structural configuration of metamaterials by using mechanical stretching and microelectromechanical system (MEMS)-based techniques (Cong et al., 2017; Pitchappa et al., 2016; Xu and Lin, 2018; Zhu et al., 2011). Herein, the MEMS-based tuning mechanism can serve as a perfect platform to modify the structural configuration and electromagnetic properties of metamaterial. Although an all-optical network is the development tendency of the future optical communication, opto-logic operating devices with high compatibility are desired. MEMS-based metamaterials have been demonstrated to realize optical reconfigurable characteristics, which can represent the logic bits and exhibit great prospects in optical programmable applications (Fu et al., 2011; Liao and Lin, 2020; Ma et al., 2014).

Because the large geometrical deformation of metamaterials can be realized by using mechanical stretching method, the uses of flexible substrates to tune the electromagnetic responses of

[1]School of Electronics and Information Technology, Sun Yat-Sen University, Guangzhou 510006, China

[2]Lead contact

*Correspondence: linyoush@mail.sysu.edu.cn

https://doi.org/10.1016/j.isci.2022.104072

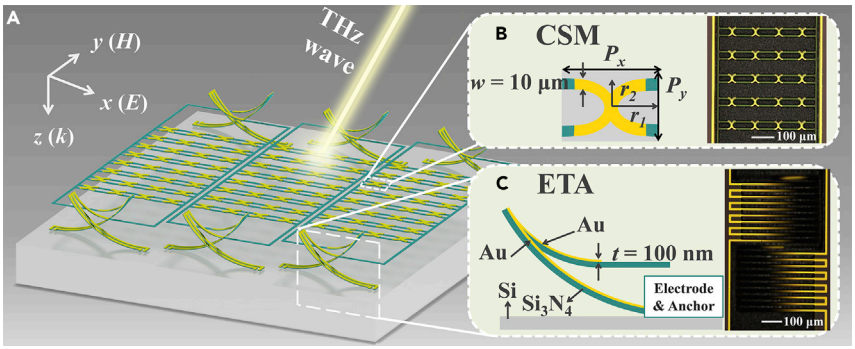

Figure 1. Schematic drawings of the opto-logic operation device

(A) MEMS-based CSM using electrothermal actuation mechanism. The inserted coordinates indicate the wave direction for transverse electric mode, where *E*, *H*, and *k* are the electric field, magnetic field, and wave vector of the incident electromagnetic wave.

(B) The periodic unit cell of CSM. The inserted image is the optical images of CSM.

(C) The configuration of ETA. The inserted image is the optical images of ETA.

metamaterials are commonly studied, including polydimethylsiloxane (PDMS), polyimide, and polyethylene terephthalate (PET) (Kim et al., 2016; Xu et al., 2018). However, poor cohesiveness and incompatibility to the semiconductor manufacturing process have hindered their large-scale application. Moreover, it is difficult to integrate the mechanical stretching method into electronic devices, although the most mature and practical technology in our daily life is using electric signals. In this study, a MEMS-based tunable metamaterial is proposed to realize opto-logic function in the THz frequency range by integrating cross-shaped metamaterial (CSM) on MEMS-based electrothermal actuator (ETA) platform. In this study, a MEMS-based tunable metamaterial is proposed to realize opto-logic function in the THz frequency range by integrating cross-shaped metamaterial (CSM) on MEMS-based electrothermal actuator (ETA) platform. The proposed MEMS-based CSM device can be tuned by mechanically stretching on silicon (Si) substrate to overcome the limitations of stretchable metamaterial on flexible substrate. A large tuning range of 0.54 THz is realized by driving a direct current (DC) bias voltage of 0.20 V on MEMS-based CSM devices. By monitoring the emission and detection of MEMS-based CSM devices at 1.20 THz, it exhibits a "XNOR" logic gate function corresponding to the electric signal input and optical output. This proposed actively tunable approach paves a new way toward voltage-controllable metamaterials, which is suitable for widespread applications in THz frequency range, such as logical operation, optical communication, signal detection, and so on.

RESULTS

Metamaterial design

Figure 1 illustrates the schematic diagram of MEMS-based CSM device for THz opto-logic operation. The proposed device is composed of periodic meta-atoms and an ETA platform. The material of meta-atoms is gold (Au) layer and that of ETAs is the composition of Au and silicon nitride (Si_3N_4) layers on Si substrate. The thickness of Si substrate is 500 μm. Each meta-atom of CSM consists of two half-elliptic-rings to form an approximate cross shape. The incident light is assumed to be a plane wave. In the plane wave system, the E-vector is fixed along the direction of the x axis, whereas the H-vector is fixed along the direction of the y axis. They are perpendicular to each other in the *x*-*y* plane. The *k*-vector is fixed along the *z* axis's direction. The period geometry of metamaterial greatly affects the resonant frequency and the period under the hundred-micron scale can provide the optical response operating at the THz frequency range. To enable the generation of electromagnetic resonance in the THz frequency range, the periods of CSM along the x axis and the *y* axis directions are fixed as 115 and 100 μm, i.e., P_x = 115 μm and P_y = 100 μm, respectively. The metamaterial thickness (*t*) is 100 nm and the area of the periodic array is 2 × 2 mm. CSM structures are connected with the ETA platform by using a Si_3N_4 frame. The length and line width of ETA are kept as constant as 360 and 10 μm, respectively. ETAs are fully released and then deformed upward after isotropically undercutting Si substrate owing to the difference in thermal expansion coefficients between Au and Si_3N_4 layers. Although the cantilevers and frame are both composed of Au and Si_3N_4 layers, the deformation of the device is completely determined by the

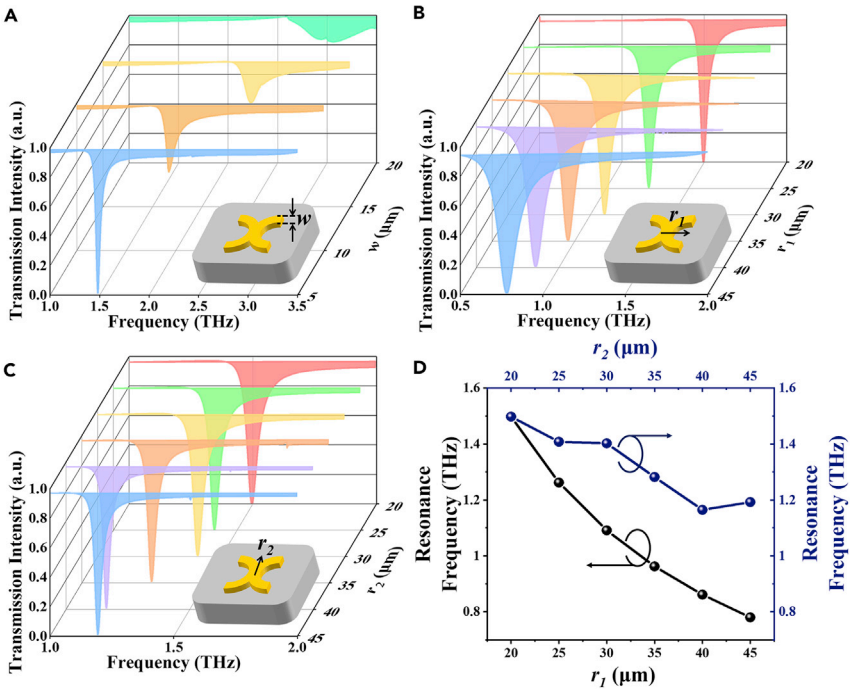

Figure 2. The electromagnetic properties of CSM device under different geometrical dimensions

(A–C) Transmission spectra of CSM with different line widths (w), transverse radius (r_1), and longitudinal radius (r_2) values, respectively.

(D) Relationships of resonance frequency to r_1 and r_2 values of CSM.

characteristics of these two materials. CSM structures will be elevated and can be stretched by driving a DC bias voltage on ETAs. The larger thermal expansion coefficient of Au layer provides tensile residual stress and the smaller thermal expansion coefficient of Si_3N_4 layer provides compressive residual stress through the fabrication processes. The radius of curvature and bending height of ETAs are determined by their geometric dimension, e.g., length and thickness (Shavezipur et al., 2012). Therefore, the initial released bending height of ETAs can be precisely controlled by tailoring the suitable length and the thickness of Au and Si_3N_4 layers. Owing to the Si_3N_4 insulated layer and rough Si substrate, the proposed tunable CSM platform can prevent the MEMS cantilevers from snapping down on Si surface. Such MEMS cantilevers can be reversibly bent up and downward to effectively avoid the irreversible damages to the entire device, which means that the proposed design is promising to be more stable and reconfigurable compared with other logic operation platforms (Manjappa et al., 2018; Zhang et al., 2020a, 2020b). The power consumption of CSM devices can be greatly reduced because of the low driving-voltage of 0.1 V. In addition, because the large geometrical deformations of the metamaterial are proved to provide a large tuning range for the metamaterial, the proposed MEMS-based CSM device can serve as a perfect logic operation platform to mechanically stretch these metamaterials on the Si substrate. The various kinds of metamaterials can be designed on the ETA platform to further expand the operating frequency range. Owing to such characteristics, a CSM device exhibits more flexibility in the logic operation application. This proposed actively tunable approach paves a new way toward voltage-controllable metamaterials with a large tuning frequency range to satisfy various requirements of real applications. By driving a DC bias voltage on the electrodes of ETAs, the resistance heat is induced by the current flow and then increases the temperature within ETAs. The elevated ETAs are recoverable to bend downwards and upwards, which provides the three-dimensional displacement, including horizontal and vertical displacements. Herein, the horizontal displacement of ETAs facilitates the deformation of CSM to change the P_x value. The inserted images in Figures 1B and 1C show the optical images of CSM and ETA, respectively. It can be clearly observed that the ETAs are fully released from the blurred the region in the optical image. Such a design provides an effective strategy to exploit the displacement along different directions and enlarge the tuning range of metamaterials in the three-dimensional free space.

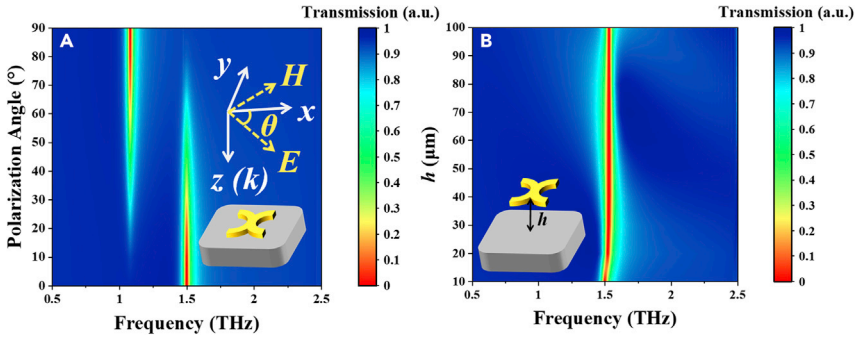

Figure 3. The electromagnetic properties of CSM device under different tunable configuration

(A and B) Transmission spectra of CSM with different polarization angles (θ) and height (H) values, respectively.

Electromagnetic properties

To figure out the optimized CSM design, various geometric dimensions of CSM are compared and discussed as shown in Figure 2. CSM is designed to exhibit different effective permittivity and permeability under different compositions of unit cells. The effective permittivity (ε_{eff}) and permeability (μ_{eff}) of CSM can be calculated as (Smith et al., 2005).

$$\varepsilon_{eff} = n_{eff}/z_{eff} \quad \text{(Equation 1)}$$

$$\mu_{eff} = n_{eff} z_{eff} \quad \text{(Equation 2)}$$

$$n_{eff} = \frac{1}{kt}\cos^{-1}\left(\frac{1-\beta^2+\gamma^2}{2t}\right) \quad \text{(Equation 3)}$$

$$z_{eff} = \sqrt{\frac{(1+\beta)^2-\gamma^2}{(1+\beta)^2-\gamma^2}} \quad \text{(Equation 4)}$$

where n_{eff} and z_{eff} are effective refraction index and impedance index of CSM, respectively, k is the incident wave vector, t is the metamaterial thickness, β is the reflection coefficient, and γ is the transmission coefficient. The periodic meta-atom of CSM exhibits three key parameters. They are line widths (w), transverse radius (r_1), and longitudinal radius (r_2), respectively. Figure 2A shows the transmission spectra of CSM with different w values under the condition of $r_1 = r_2 = 20$ μm. By increasing w value, the resonance becomes broader and the transmission intensity decreases from 1.0 to 0.2, which means the resonance becomes weaker. The optimized w parameter is 5 μm, which is kept as constant in this study. The transmission spectra of CSM with different r_1 and r_2 values are illustrated in Figures 2B and 2C. The resonant intensities are 1.0 to realize perfect zero-transmission. The operating resonances are summarized in Figure 2D. The resonances are red-shifted from 1.50 THz to 0.78 THz by increasing r_1 value from 20 μm to 45 μm and are red-shifted from 1.50 THz to 1.19 THz by increasing r_2 value from 20 μm to 45 μm. The tuning ranges of CSM are 0.72 THz and 0.31 THz, respectively. These results provide a strategy to deform CSM along x axis and y axis directions with large tuning ranges for the realization of THz-wave optoelectronic applications.

Figure 3A shows the transmission spectra of CSM with different polarization angles (θ). θ value is defined as the included angle of x axis direction and E-field direction as illustrated in the inserted schematic of Figure 3A. By increasing θ to 90°, the E-vector is gradually modified to be along y axis direction, whereas the H-vector is gradually modified to be along x axis direction. The geometrical parameters of CSM are kept as constant as $w = 5$ μm and $r_1 = r_2 = 20$ μm in the following discussions. CSM structure is an asymmetric structure, which exhibits polarization-dependent characteristics. At the condition of $\theta = 0°$, the resonance of CSM is at 1.50 THz. It will decay by increasing θ value and then generate a second-order resonance at 1.08 THz. By continuously increasing θ value to 90°, the resonance of CSM is changed at 1.08 THz. The resonance of CSM can be tuned and switched between 1.50 THz and 1.08 THz by changing incident θ value for single-resonance and dual-resonance applications. Although CSM is released to elevate with a height (h) from substrate, the electromagnetic responses of CSM are essential to evaluate the influences of dynamic motion. Herein, the condition of $\theta = 0°$ represents the transverse electric (TE) mode, whereas the condition of $\theta = 90°$ represents the transverse magnetic (TM) mode. Figure 3B shows the transmission spectra of CSM with different h values at TE mode. It can be clearly observed that the variation of resonance

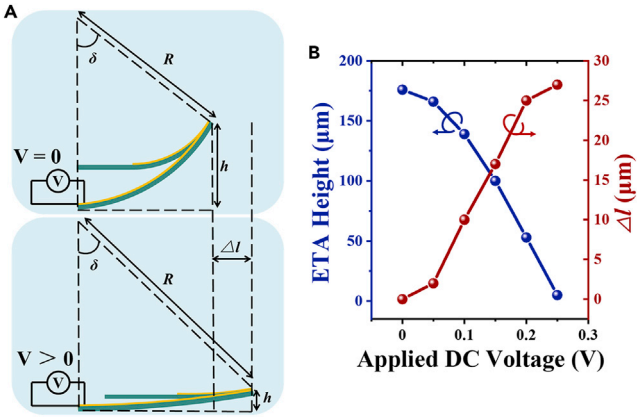

Figure 4. Actuation mechanism of ETA

(A) Schematic drawings of ETA in the cross-section with and without a driving voltage.

(B) Relationships of driving voltages to vertical and horizontal deformations.

is negligible by changing *h* value from 10 μm to 100 μm, which means that the resonance of the metamaterial pattern is uncoupled with the silicon substrate after being released. Such CSM design can provide the stable optical output signals with high robustness under the releasing or suspending state.

Actuation mechanism

The difference of thermal expansion coefficients between Au and Si_3N_4 layers determines ETAs can be driven to bend downwards by applying a DC bias voltage. It will generate a horizontal displacement (Δl) as shown in Figure 4A. Such a horizontal displacement of ETA is induced by the change in the radius of curvature. The corresponding relationship between the deformed the radius of curvature (R) and height of ETA (h) is shown in Figure 4, which can be expressed by the following formula.

$$L = 2\pi R \times (\delta / 360^{\circ}) \quad \text{(Equation 5)}$$

$$\cos\delta = (R - h)/R \quad \text{(Equation 6)}$$

where L is the ETA length and δ is the center angle. For the radius of curvature, it can be certainly determined by the deformed height of ETA as the ETA length is kept at a constant of 360 μm. Thus, the deformed height of ETA is adopted to describe the actuating state of ETA. Figure 4B shows the nonlinear relationships between applied DC bias voltages and deformations along both vertical and horizontal directions. By increasing DC voltage from 0 V to 0.3 V, the ETA height decreases from 176 μm to 5 μm, whereas Δl increases from 0 μm to 27 μm. Such ETA characteristics are suitable to be implanted into the actively tunable CSM with a large displacement.

The integration of ETAs and CSM provides the possibility to control the deformation of metamaterials by driving a DC bias voltage. Figure 5A shows the schematic drawings of MEMS-based CSM with and without a driving voltage, respectively. By applying DC voltage, the deformed height (h) can be actuated from 176 μm to 5 μm. The driving voltages are applied on the ETAs to generate electric current and resistance heat. Each driving DC bias voltage makes ETAs bend downward and then provides the CSM array with a horizontal deformation. The inserted images of Figure 5A indicate the change of CSM unit cell by driving a DC bias voltage, i.e., the deformations of r_1 and r_2 values. The relationships of applied DC voltages to r_1 and r_2 values are plotted in Figure 5B. By increasing the applied DC voltage, r_1 decreases from 33.3 μm to 20.1 μm, whereas r_2 increases from 12.6 μm to 19.7 μm. The trends are nonlinear and are identical to the ETA formula expressed by (Shavezipur et al., 2012)

$$\frac{1}{R} = \frac{1}{C}\left[\Delta T(\alpha_1 - \alpha_2) - \left(\frac{1}{E_1} + \frac{1}{E_2}\right)\frac{2F_x(L-x)}{A(d_1+d_1)}\right] \quad \text{(Equation 7)}$$

$$C = 2\frac{E_1 I_1 + E_2 I_2}{A(d_1+d_2)}\left(\frac{1}{E_1} + \frac{1}{E_2}\right) + \frac{d_1+d_2}{2} \quad \text{(Equation 8)}$$

$$F_x = \frac{\varepsilon_0 A}{2(h-x)^2} V^2 \quad \text{(Equation 9)}$$

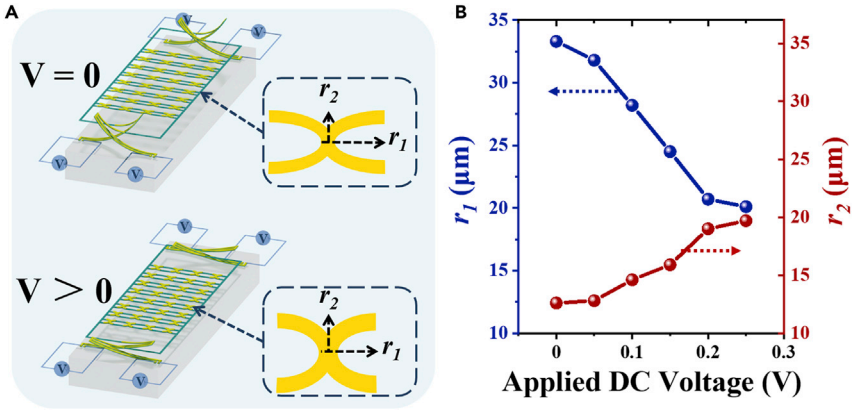

Figure 5. Electrothermal actuation mechanism for the integrated CSM device

(A) 3D Schematic drawings of MEMS-based CSM devices with and without a driving voltage.

(B) Relationships of driving voltages to transverse radius (r_1) and longitudinal radius (r_2) values.

$$\Delta T \propto Q \propto V^2 \quad \text{(Equation 10)}$$

where R and h are the radius of curvature and deformed height of the ETA, respectively, ΔT is the variation of heating temperature, E is the Young's modulus, α is the thermal expansion coefficient, L is the length of the ETA, x is the vertical displacement induced by an applied DC bias voltage (V), A is the area, d is the layer thickness, I is the area moment of inertia, and Q is the resistance heat generated by the following current. The subscript 1 and 2 represent different materials, which are Si_3N_4 and Au materials in the ETA design, respectively. According to such a relationship between the applied DC bias voltage and the deformed height, the horizontal displacement of the ETA can be calculated by referring to the relationships as shown in Figure 4A.

The tunable optical properties of MEMS-based CSM devices are investigated by changing the periodicity of CSM along the direction of the x axis. The schematics of stretchable CSM devices are shown in Figure 6A. Each column of the CSM array is composed of four CSM unit cells. The periodic column is denoted as $P_{total} = 4P_0 = 460$ μm, where P_0 is the initial CSM period. The period of each unit cell decreases, whereas the total period of four-unit cells remains constant. Figure 6B shows the effects on the transmission spectra. Although the change of period is much smaller than the total period, there is little variation. In these proposed designs, p value is larger than 100 μm by driving 0.25 V. These results indicate that the aperiodic effect can be neglected in this work. The transmission spectra of MEMS-based CSM with different driving DC bias voltages in TE mode are shown in Figure 6B. By driving a voltage of 0.2 V, the resonances are blue-shifted from 1.04 THz to 1.58 THz with a perfect zero-transmission. The tuning range is 0.54 THz. Moreover, the resonances are red-shifted back to 1.50 THz by driving a voltage of 0.25 V. Figure 6C shows a similar result for CSM in TM mode. By driving a voltage of 0.20 V, the resonances are blue-shifted from 0.86 THz to 1.12 THz with a perfect zero-transmission. Afterward, these resonances are red-shifted back to 1.08 THz by driving a voltage of 0.25 V. Compared with the resonances in TE mode, the resonances of CSM in TM mode exhibit a smaller tuning range of 0.36 THz, but the full width at half maxima (FWHM) is narrower. It means that the tunable CSM can be operated with diverse optical performance by modifying the polarization state for different requirements.

Logic gate operation function

By exploiting the voltage-controllable optical properties, CSM can perform widespread functions, such as logic modulation and operation. The programmable functions of THz opto-logic operation of CSM are shown in Figure 7A. A THz laser is adopted to induce the unmodulated THz wave while two power suppliers are contracted to provide the total electrical inputs on the CSM device. They are defined as V_1 and V_2, respectively. The operating frequency of THz laser is 1.2 THz and the output signal is polarized to meet the requirement of TE mode. By applying such electrical signal inputs, the transmission spectra of MEMS-based CSM devices can be modified, which means the electrical signals are converted into optical signals. The change of output signals under different conditions is indicated in Figure 7B. The THz signal

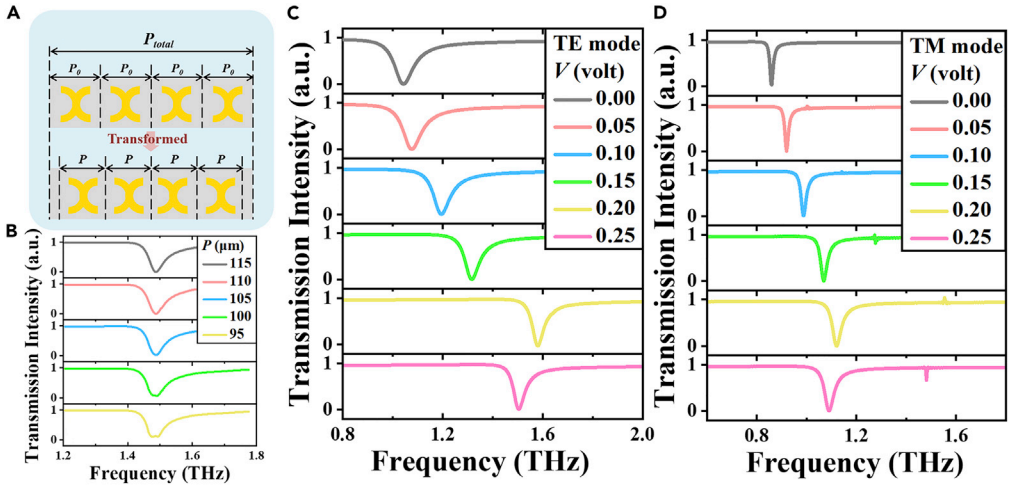

Figure 6. The electromagnetic properties of the CSM device by applying different excitations

(A and B) 2D Schematic drawing and deformed effect of MEMS-based CSM device, respectively.

(C and D) Transmission spectra of MEMS-based CSM device with different driving DC voltages in TE and TM modes, respectively.

output is detected at 1.20 THz and the input signal is switched between 0 and 0.1 V. The transmission intensity of CSM is 0.81 without any electrical signal input, whereas it is 0.97 at the condition of $V_1 = V_2 = 0.1$ V. Such a THz wave is propagated through the CSM device with a high efficiency, which could be referred to as the "on" state for logic operating function. Meanwhile, the transmission intensity sharply dropped to 0.001 under the conditions of $V_1 = 0$ V, $V_2 = 0.1$ V, $V_1 = 0.1$ V, $V_2 = 0$ V. The electromagnetic resonance is strongest at 1.20 THz and the incident THz wave cannot be propagated through the CSM device at such states, which could be referred to as an "off" state for logic operating function. These results of CSM devices realize the "XNOR" logic gate operation function as illustrated in Figure 7C. "XNOR" logic gate is a key component in the conventional logic integrated circuit (IC). However, the advanced development of an all-optical logic network is limited by the lack of an integrable "XNOR" logic gates. The proposed designs provide a strategy to perform "XNOR" logic gate function with high efficiency and will be a breakthrough in the development of an all-optical logic network. Moreover, the proposed CSM is used to demonstrate and provide a tuning response and then realize XNOR operation. Such a function is determined by the geometrical dimension and the optical properties of CSM. By properly tailoring the metamaterial pattern on the proposed MEMS-based platform of metadevice, other logic operations on the same device can be achieved.

DISCUSSION

A MEMS-based tunable metadevice is proposed for THz opto-logic operation by integrating MEMS ETAs and CSM. The ETAs are initially bent upward owing to the difference in thermal expansion coefficients between Au and Si_3N_4 layers through MEMS fabrication process. By driving a DC bias voltage, the released ETAs can be recovered to bend downward and provide a horizontal displacement to make the deformation of CSM and then control the THz wave propagation. The geometric dimension of CSM is optimized to exhibit different operating frequencies. The pre-bent ETAs can realize a displacement of 27 μm by driving a voltage of 0.25 V. Such an actuation induces a large deformation on the integrated CSM device, which can achieve a tuning range of 0.54 THz in TE mode and 0.36 THz in TM mode. Although MEMS-based CSM devices can be switched between "on" and "off" states, the proposed designs exhibit "XNOR" logic gate function and are promising to serve as a key component in an all-optical logic network. In view of these voltage-controllable characterizations, MEMS-based CSM devices could be further used in widespread applications, such as opto-logic operating, high-efficient optical switching, 3D imaging, and actively tunable sensing.

Limitations of the study

The main limitation for the development of ETA-based CSM devices is the slow actuating response speed. Such methods induce the resistance heat by the current flow and then increase the temperature within

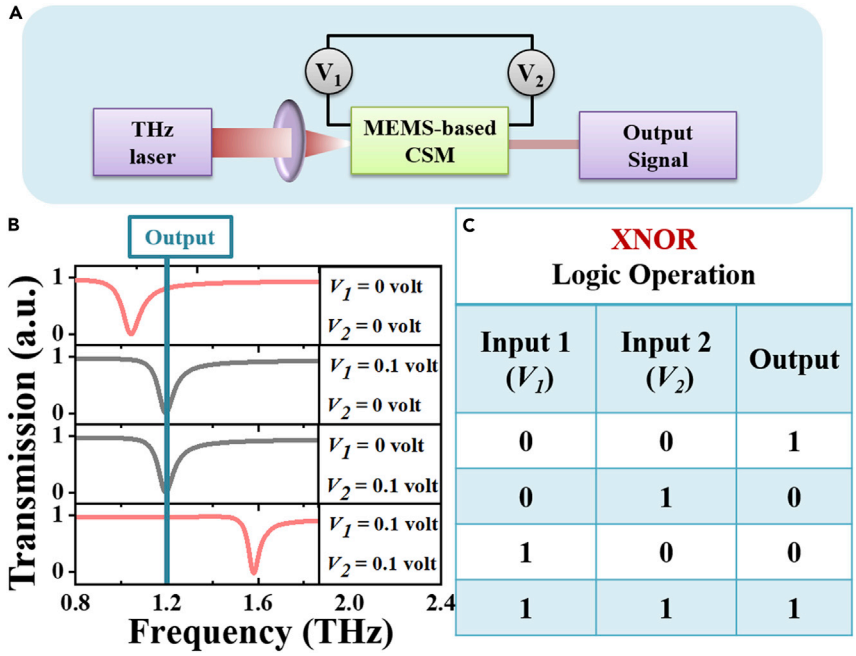

Figure 7. Dual-input logic gate operation function achieved by the CSM device

(A) Schematic of THz opto-logic operation of MEMS-based CSM.

(B) Transmission responses of MEMS-based CSM under the conditions of $V_1 = V_2 = 0$ V, $V_1 = 0.1$ V and $V_2 = 0$ V, $V_1 = 0$ V and $V_2 = 0.1$ V, $V_1 = V_2 = 0.1$ V, respectively. The output signal is observed at 1.20 THz.

(C) "XNOR" logic gate operation function performed by MEMS-based CSM.

ETAs. The rise and fall of temperature takes time during the repeatedly driving process, which limits the response speed of devices. This problem remains open and will be realized in future work.

STAR★METHODS

Detailed methods are provided in the online version of this paper and include the following:

- KEY RESOURCES TABLE
- RESOURCE AVAILABILITY
  - Lead contact
  - Materials availability
  - Data and code availability
- EXPERIMENTAL MODEL AND SUBJECT DETAILS
- METHOD DETAILS
  - 3D-FDTD numerical method
  - COMSOL thermal and mechanical simulation
- QUANTIFICATION AND STATISTICAL ANALYSIS
- ADDITIONAL RESOURCES

ACKNOWLEDGMENTS

The authors acknowledge the financial support from research grants of Natural Science Foundation of Basic and Applied Foundation of Guangdong Province (2021A1515012217), National Key Research and Development Program of China (2019YFA0705004), National Natural Science Foundation of China (11690031), and the State Key Laboratory of Optoelectronic Materials and Technologies of Sun Yat-Sen University for the use of experimental equipment.

AUTHOR CONTRIBUTIONS

X.X., R.X., and Y-S.L. conducted the methodology. R.X. conducted the software and the experiment. R.X. drew the schematic diagrams in the paper. X.X. and R. X. led the writing of original draft preparation. X.X.

and Y-S.L. led the review and editing of the paper. All authors discussed the results and commented on the manuscript.

DECLARATION OF INTERESTS

The authors declare no competing interests.

Received: December 1, 2021
Revised: February 16, 2022
Accepted: March 11, 2022
Published: April 15, 2022

REFERENCES

Chen, H.T., Padilla, W.J., Cich, M.J., Azad, A.K., Averitt, R.D., and Taylor, A.J. (2009). A metamaterial solid-state terahertz phase modulator. Nat. Photon. *3*, 148–151.

Chen, H.T., Yang, H., Singh, R., O'Hara, J.F., Azad, A.K., Trugman, S.A., Jia, Q.X., and Taylor, A.J. (2010). Tuning the resonance in high-temperature superconducting terahertz metamaterials. Phys. Rev. Lett. *105*, 247402.

Cong, L.Q., Pitchappa, P., Lee, C., and Singh, R. (2017). Active phase transition via loss engineering in a terahertz MEMS metamaterial. Adv. Mater. *29*, 1700733–1700733.

Das, B., Yun, H.S., Park, N., Jeong, J., and Kim, D.S. (2021). A transformative metasurface based on zerogap embedded template. Adv. Opt. Mater. *9*, 2002164.

Fu, Y.H., Liu, A.Q., Zhu, W.M., Zhang, X.M., Tsai, D.P., Zhang, J.B., Mei, T., Tao, J.F., Guo, H.C., Zhang, X.H., et al. (2011). A micromachined reconfigurable metamaterial via reconfiguration of asymmetric split-ring resonators. Adv. Funct. Mater. *21*, 3589–3594.

Kenanakis, G., Zhao, R., Katsarakis, N., Kafesaki, M., Soukoulis, C.M., and Economou, E.N. (2014). Optically controllable THz chiral metamaterials. Opt. Express *22*, 12149–12159.

Kim, D., Yun, H.S., Das, B., Rhie, J., Vasa, P., Kim, Y.I., Choa, S.H., Park, N., Lee, D., Bahk, Y.M., et al. (2021). Topology-changing broadband metamaterials enabled by closable nanotrenches. Nano Lett. *21*, 4202–4208.

Kim, K., Lee, D., Eom, S., and Lim, S. (2016). Stretchable metamaterial absorber using liquid metal-filled polydimethylsiloxane (PDMS). Sensors *16*, 521.

Landy, N.I., Sajuyigbe, S., Mock, J.J., Smith, D.R., and Padilla, W.J. (2008). Perfect metamaterial absorber. Phys. Rev. Lett. *100*, 207402.

Lee, S.H., Choi, M., Kim, T.T., Lee, S., Liu, M., Yin, X., Choi, H.K., Lee, S.S., Choi, C.G., Choi, S.Y., et al. (2012). Switching terahertz waves with gate-controlled active graphene metamaterials. Nat. Mater. *11*, 936–941.

Liao, Y.H., and Lin, Y.S. (2020). Reconfigurable terahertz metamaterial using split-ring meta-atoms with multifunctional electromagnetic characteristics. Appl. Sci. *10* (15), 5267–5267.

Liu, M.K., Hwang, H.Y., Tao, H., Strikwerda, A.C., Fan, K.B., Keiser, G.R., Sternbach, A.J., West, K.G., Kittiwatanakul, S., Lu, J.W., et al. (2012). Terahertz-field-induced insulator-to-metal transition in vanadium dioxide metamaterial. Nature *487*, 345–348.

Liu, N., Weiss, T., Mesch, M., Langguth, L., Eigenthaler, U., Hirscher, M., Sonnichsen, C., and Giessen, H. (2010). Planar metamaterial analogue of electromagnetically induced transparency for plasmonic sensing. Nano Lett. *10*, 1103–1107.

Ma, F.S., Lin, Y.S., Zhang, X.H., and Lee, C. (2014). Tunable multiband terahertz metamaterials using a reconfigurable electric split-ring resonator array. Light-sci. Appl. *3*, e171.

Ma, H.F., and Cui, T.J. (2010). Three-dimensional broadband ground-plane cloak made of metamaterials. Nat. Commun. *1*, 1–6.

Manjappa, M., Pitchappa, P., Singh, N., Wang, N., Zheludev, N.I., Lee, C., and Singh, R. (2018). Reconfigurable MEMS Fano metasurfaces with multiple-input-output states for logic operations at terahertz frequencies. Nat. Commun. *9*, 4056.

Pitchappa, P., Manjappa, M., Ho, C.P., Singh, R., Singh, N., and Lee, C. (2016). Active control of electromagnetically induced transparency analog in terahertz MEMS metamaterial. Adv. Opt. Mater. *4*, 541–547.

Shavezipur, M., Gou, W.J., Carraro, C., and Maboudian, R. (2012). Characterization of adhesion force in MEMS at high temperature using thermally actuated microstructures. J. Microelectromech. S. *21*, 541–548.

Smith, D.R., Vier, D.C., Koschny, T., and Soukoulis, C.M. (2005). Electromagnetic parameter retrieval from inhomogeneous metamaterials. Phys. Rev. E. *71*, 036617.

Tao, H., Landy, N.I., Bingham, C.M., Zhang, X., Averitt, R.D., and Padilla, W.J. (2008). A metamaterial absorber for the terahertz regime: design, fabrication and characterization. Opt. Express *16*, 7181–7188.

Xu, R.J., and Lin, Y.S. (2018). Characterizations of reconfigurable infrared metamaterial absorbers. Opt. Lett. *43*, 4783–4786.

Xu, Z.F., and Lin, Y.S. (2019). A stretchable terahertz parabolic-shaped metamaterial. Adv. Opt. Mater. *7* (19), 1900379–1900379.

Xu, R.J., and Lin, Y.S. (2020). Tunable infrared metamaterial emitter for gas sensing application. Nanomaterials *10*, 1442.

Xu, R.J., Luo, J., Sha, J., Zhong, J.T., Xu, Z.F., Tong, Y.L., and Lin, Y.S. (2018). Stretchable IR metamaterial with ultra-narrowband perfect absorption. Appl. Phys. Lett. *113*, 101907.

Xu, T., Xu, R.J., and Lin, Y.S. (2020). Tunable terahertz metamaterial using electrostatically electric split-ring resonator. Results Phys. *19*, 103638.

Zhang, X.G., Jiang, W.X., and Cui, T.J. (2018a). Frequency-dependent transmission-type digital coding metasurface controlled by light intensity. Appl. Phys. Lett. *113*, 091601.

Zhang, X.G., Tang, W.X., Jiang, W.X., Bai, G.D., Tang, J., Bai, L., Qiu, C.W., and Cui, T.J. (2018b). Light-controllable digital coding metasurfaces. Adv. Sci. *5*, 1801028.

Zhang, X.G., Jiang, W.X., Jiang, H.L., Wang, Q., Tian, H.W., Bai, L., Luo, Z.J., Sun, S., Luo, Y., Qiu, C.W., et al. (2020a). An optically driven digital metasurface for programming electromagnetic functions. Nat. Electron. *3*, 165–171.

Zhang, X.G., Yu, Q., Jiang, W.X., Sun, Y.L., Bai, L., Wang, Q., Qiu, C.W., and Cui, T.J. (2020b). Polarization-controlled dual-programmable metasurfaces. Adv. Sci. *7*, 1903382.

Zheng, D.Y., and Lin, Y.S. (2020). Tunable dual-split-disk resonator with electromagnetically induced transparency characteristic. Adv. Mater. Technol. *5* (11), 2000584–2000584.

Zhu, W.M., Liu, A.Q., Zhang, X.M., Tsai, D.P., Bourouina, T., Teng, J.H., Zhang, X.H., Guo, H.C., Tanoto, H., Mei, T., et al. (2011). Switchable magnetic metamaterials using micromachining processes. Adv. Mater. *23*, 1792.

STAR★METHODS

KEY RESOURCES TABLE

REAGENT or RESOURCE	SOURCE	IDENTIFIER
Software and algorithms		
FDTD	Lumerical Co	https://www.lumerical.com/products/fdtd/
COMSOL Multiphysics 5.5	COMSOL Inc	https://www.comsol.com

RESOURCE AVAILABILITY

Lead contact

Further information and requests for resources and reagents should be directed to and will be fulfilled by the lead contact, Yu-Sheng Lin (linyoush@mail.sysu.edu.cn).

Materials availability

This study did not generate new unique reagents.

Data and code availability

- All data reported in this paper will be shared by the lead contact upon request.
- No new code was generated during the course of this study.
- Any additional information required to reanalyze the data reported in this paper is available from the lead contact upon request.

EXPERIMENTAL MODEL AND SUBJECT DETAILS

The three-dimensional finite-difference time-domain (FDTD) method is employed to analyze the electromagnetic performance of the proposed CSM devices. In these numerical simulations, the propagation direction of incident wave is set to be perpendicular to the x-y plane where the MEMS-based metamaterial pattern array lies. Additionally, the periodic boundary conditions are set in the x- and y axis directions while the perfectly matched layer (PML) boundaries conditions are set in the z axis direction.

METHOD DETAILS

3D-FDTD numerical method

With the numerical model, the electromagnetic properties can be calculated. By setting the monitors on backside of device, the transmission spectra of the incident electromagnetic wave are calculated to observe the resonant intensity.

COMSOL thermal and mechanical simulation

The ETA platform simulation in this study was performed by finite element modeling (FEM) in the software COMSOL Multiphysics. The thermal expansion deformation (ϵ) of CSM device was calculated by

$$\varepsilon = \alpha(T)(T - T_{ref}),$$

where $\alpha(T)$ is the coefficient of thermal expansion (α_{Au} = 14.2 ppm K^{-1} and α_{Si3N4} = 4.0 ppm K^{-1} at room temperature) and T_{ref} is the referred temperature (300 K). The temperature (T) of CSM device was calculated by

$$\rho c_p u \cdot \nabla T = \nabla \cdot (k \nabla T) + Q_e,$$
$$Q_e = J \cdot E,$$

where ρ is the density (ρ_{Au} = 19320 kg/m^3, ρ_{Si3N4} = 3440 kg/m^3), C_p is the specific heat capacity (C_{Au} = 0.13 kJ $kg^{-1}\cdot K^{-1}$, C_{Si3N4} = 0.71 kJ $kg^{-1}\cdot K^{-1}$), u is the displacement, Q_e is the Joule heat, J is the current volume density vector, E is the electric field intensity vector.

QUANTIFICATION AND STATISTICAL ANALYSIS

The simulation data is produced by FDTD and COMSOL software from the numerical model. Figures were produced by Origin from the raw data.

ADDITIONAL RESOURCES

Any additional information about the simulation and data reported in this paper is available from the lead contact on request.